Search for neutrinoless double-electron capture of ^{156}Dy

S. W. Finch and W. Tornow

Phys. Rev. C **92**, 065503 — Published 31 December 2015

DOI: 10.1103/PhysRevC.92.065503

Search for neutrinoless double-electron capture of ^{156}Dy

S.W. Finch* and W. Tornow
Department of Physics, Duke University, Durham, North Carolina 27708, USA
and Triangle Universities Nuclear Laboratory, Durham, North Carolina 27708, USA

Background: Multiple large collaborations are currently searching for neutrinoless double-β decay, with the ultimate goal of differentiating the Majorana-Dirac nature of the neutrino.

Purpose: Investigate the feasibility of resonant neutrinoless double-electron capture, an experimental alternative to neutrinoless double-β decay.

Method: Two clover germanium detectors were operated underground in coincidence to search for the de-excitation γ rays of ^{156}Gd following the neutrinoless double-electron capture of ^{156}Dy. 231.95 days of data were collected at the Kimballton underground research facility with a 231.57 mg enriched ^{156}Dy sample.

Results: No counts were seen above background and half-life limits are set at $O(10^{16} - 10^{18})$ yr for the various decay modes of ^{156}Dy.

Conclusion: Low background spectra were efficiently collected in the search for neutrinoless double-electron capture of ^{156}Dy, although the low natural abundance and associated lack of large quantities of enriched samples hinders the experimental reach.

I. INTRODUCTION

Neutrinoless double electron capture ($0\nu ECEC$) is a second-order weak nuclear decay and a possible experimental alternative to neutrinoless double-β ($0\nu\beta\beta$) decay [1]. Observation of either of these two decays would provide evidence that the neutrino has a Majorana mass component, as opposed to a purely Dirac mass. In $0\nu ECEC$, the nucleus will absorb two atomic electrons, lowering its nuclear charge by two, with the emission of no particles. This decay will then proceed if an excited state in the daughter nucleus is degenerate with the Q value of the decay, as a means to dissipate the excess energy [2]. Furthermore, the wave-function overlap of the parent and excited state of the daughter nucleus leads to a resonant enhancement effect, decreasing the expected half-life [3]. The decay rate for $0\nu ECEC$ may be calculated as

$$\lambda^{0\nu} = g_A^4 G_{0\nu} |M^{0\nu}|^2 \langle m_\nu \rangle^2 \frac{\Gamma}{\Delta^2 + \frac{1}{4}\Gamma^2}, \tag{1}$$

where $G_{0\nu}$ is a prefactor containing the electron-nucleus wave-function overlap, $M^{0\nu}$ is the transition nuclear matrix element, $\langle m_\nu \rangle$ is the Majorana neutrino mass, and the remaining terms constitute the resonant enhancement factor, where Δ is the degeneracy parameter (0 keV for complete degeneracy) and Γ is the combined width of the states [4].

For this decay to be a valid experiment alternative to $0\nu\beta\beta$ decay, a candidate nucleus exhibiting the parent-daughter degeneracy must exist. Recent precision mass measurements identified ^{156}Dy as the current best candidate for resonant $ECEC$ [5]. Reference [5] identified four possible states in ^{156}Gd which are degenerate to within 1.37 keV (depending on the shell of the capturing electron); these are given in Table I. The 2_6^+ state in ^{156}Gd has the possibility of a complete degeneracy, within experimental uncertainties, which would produce an enhancement factor of 10^{10}. Unfortunately, this decay mode is hindered by the unlikely capture of M and N shell electrons.

TABLE I. The possible resonant transitions in ^{156}Gd for a $0\nu ECEC$ decay of ^{156}Dy. The orbitals of the capturing electrons, calculated degeneracy parameter Δ, and the enhancement factor in the rate relative to the ground state transition, EF, are given [5].

E* keV	I^π	e$^-$ orbitals	Δ keV	EF
1946.375	1_2^-	KL_1	0.75 (10)	4.1×10^6
1952.385	0_0^-	KM_1	1.37 (10)	1.7×10^6
1988.5	0_4^+	L_1L_1	0.54 (24)	2.5×10^6
2003.749	2_6^+	M_1N_3	0.04 (24)	7.7×10^8

II. EXPERIMENTAL METHOD

Following resonant double-electron capture, the daughter nucleus is left in an excited nuclear state. The nucleus will then de-excite to the ground state via γ-ray emission. Often, multiple γ rays will be emitted in coincidence. Our detection technique is based around detecting these γ rays in coincidence in order to significantly reduce the experimental background. We have previously implemented this technique to produce results for the $2\nu\beta\beta$ decay to excited nuclear states [6–8], as well as the double-electron capture of ^{112}Sn [9]. The current detector apparatus is an upgrade to the previous system, using clover high-purity germanium (HPGe) detectors over coaxial HPGe detectors.

* sfinch@tunl.duke.edu

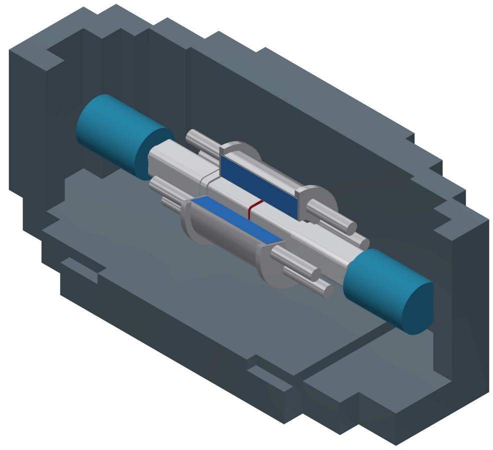

FIG. 1. (Color online) A to-scale schematic of the two clover detectors sandwiching a target in red, surrounded by the NaI annulus and lead shielding. The front lead wall and ceiling are not shown.

A. Detector apparatus

A schematic of the apparatus is shown in Fig. 1. Two clover HPGe detectors sandwich a target of interest and are surrounded by a NaI annulus and lead shielding. Clover detectors feature four coaxial-HPGe detectors (referred to as segments) sharing a common cryostat and are extensively characterized in Ref. [10]. Each crystal is 5.0 cm in diameter and 8.0 cm in length before shaping.

The NaI annulus is used as an active veto and Compton suppression shield. It measures 43.60 cm long and has a 36.83 cm exterior and 15.24 cm interior diameter. Twelve 5.08 cm PMTs, six on each side of the detector, monitor the scintillation light produced inside the detector.

The passive shielding primarily consists of a lead brick housing surrounding the detectors. The floors and side walls are shielded by 20.32 cm lead. A roof was constructed using a 123.0 × 91.5 × 2.0 cm copper plate, which supports 15.24 cm lead. The roof is extended along the length of the annulus by two 41.0 × 91.5 × 2.0 cm iron plates supporting 10.16 cm of lead. The apparatus is housed at the Kimballton Underground Research Facility (KURF), which provides 1450 meters of water equivalent shielding from cosmic rays [11].

B. Electronics and Data Acquisition system

The data-acquisition system uses NIM electronics for all signal processing and logic operations. The signals are then read and digitized by VME electronics. Each clover segment has its own preamplifier which outputs two copies of the detector signal. One copy is used for energy reconstruction. This signal is amplified by a spectroscopic amplifier then input into a 12-bit analog-to-digital (ADC) converter to record the pulse height.

The second preamplifier output is used to record the timing of the event and generate the master trigger. The eight signals are first amplified by a timing-filter amplifier, then sent through a constant-fraction discriminator (CFD). Each of these signals inputs into a time-to digital converter (TDC). The sum of all eight signals is used to generate the master trigger. It should be noted that even events below the CFD threshold are recorded as long as they are in coincidence with an event passing the CFD threshold. Given the slow trigger rate (≈ 4.5 Hz) and the short digitization time scale, the dead-time correction is minuscule.

For the NaI annulus detector, the signals from all 12 PMTs are summed, amplified, and input into the TDC. This results in a binary cut for rejecting events in coincidence with the veto.

Data acquisition is handled by C@T [12]. At every generation of the master trigger, each ADC and TDC channel are read out. The data are sent to a Linux workstation, where they are written to a file in the Continuous Electron Beam Accelerator Facility common event format. These files are then converted into a ROOT TTree using the TUNL Real-time Analysis Package [12].

C. Enriched ^{156}Dy sample

^{156}Dy suffers from an extremely low natural abundance: 0.056%. To compensate for this, two powdered oxide samples of varying enrichment were obtained from Oak Ridge National Lab. Sample No. 1 is 803.4 mg oxide enriched to 21.58% in ^{156}Dy, or 150.95 mg ^{156}Dy. Sample No. 2 is smaller: 344.3 mg oxide enriched to 20.9%, or 62.62 mg ^{156}Dy. Both samples were placed in polyethylene bags. Sample No. 1 was placed inside a 0.0089 cm thick bag with exterior dimensions 3.8 × 3.3 × 0.14 cm, and Sample No. 2 was placed inside a 0.0762 cm thick bag with dimensions of 3.5 × 2.8 × 0.165 cm. The samples were placed on top of each other inside a 0.0089 cm thick bag, resulting in a total thickness of 0.375 cm and a total mass of 213.57 mg ^{156}Dy. The samples were centered on the face of the clover detectors.

D. Data processing

New runs were started every one to five days, with an average length of three days. Two data sets were collected: one with only $^{156}Dy_2O_3$ sample No. 1 present (150.95 mg ^{156}Dy) and one with both enriched samples present (213.57 mg ^{156}Dy). These sets are referred to as data sets No. 1 and 2 respectively. Data set No. 1 contains 99.13 days of data collection and data set No. 2 contains 132.82 days of data collection.

Each individual run was closely checked for gain changes and drifts in each detector segment. Any runs in which peaks were seen to migrate by more than one channel were removed and are not included in the present analysis.

The ADC was calibrated to energy for each run using four naturally occurring background γ rays: 238.6, 511.0, 911.2, and 1460.8 keV. This calibration was done for each individual clover segment. An additional quantity, referred to as the 'addback' energy, was also calculated for each clover detector. The addback energy was calculated for events where two or more segments fired in one clover detector and is the sum of the energy deposited in those segments. A 30 keV threshold was used to determine whether or not a segment fired. This threshold was chosen to be comfortably above the 10 keV noise pedestal of the detectors and electronics while still allowing low energy Compton scatter events. Analysis showed that lowering the threshold further did not have a significant effect on the addback efficiency. In cases where only one detector segment in a clover fires, this event is recorded as the 'singles' energy.

After the clover detectors were moved underground, it was noticed that segment three of clover one, hereinafter referred to as $c13$, had an irreducible electronic noise present, decreasing the segment's resolution by a factor of ≈ 3. As such, events in which segment $c13$ triggered were removed from the present analysis. This is equivalent to using this one segment in anticoincidence.

III. ANALYSIS

The present analysis searches for coincident γ rays. When using the clover detectors, $\gamma-\gamma$ coincidences may be one of two types: internal or external. External coincidences occur when both clover detectors detect a γ-ray interaction. Internal coincidences, on the other hand, occur between two segments of the same clover detector when the other clover detector does not record any events. By searching for both internal and external coincidences, the efficiency of the $\gamma-\gamma$ coincidence technique is increased. As Compton scattering is much more likely between two adjacent segments than between the two separate clover detectors, the internal coincidence spectra have a higher background. Although the present clover detectors were not constructed to low radioactive background standards, an extremely low background region of interest (ROI) is achieved through the coincidence technique. The high Q value of $ECEC$ and high energy γ-ray transitions help to further reduce the background spectra.

Each of the four states listed in Table I, where a possible resonant decay could occur, was investigated separately. In all cases, the energy cuts used were $\pm 2\sigma$, where σ represents the detector's Gaussian energy resolution. σ was measured for each detector from the production runs using naturally occurring background peaks. A flat background was estimated using the largest peak-free region surrounding the ROI, ideally a ± 100 keV range around the ROI. The NaI annulus was used in strict anticoincidence with the clover detectors. This is the same analysis procedure as used in Ref. [8].

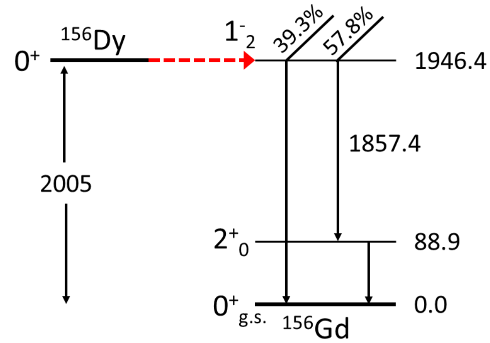

FIG. 2. (Color online) Decay scheme for the 1_2^- 1946.4 keV state of ^{156}Gd following $ECEC$ to a resonant state. Only the most intense transitions are shown, while all other transitions have a branching ratio $< 1.43\%$.

A. To the 1946.4 keV state

As can be seen in Fig. 2, the 1946.4 keV state of ^{156}Gd will primarily decay via two modes. The most intense transition creates a 1857.4 + 88.97 keV coincidence, which will be studied in this analysis. Somewhat unfortunately, the only other intense transition produces a single γ ray and is therefore not suited for the coincidence technique used in the present experiment.

Given that the 88.97 keV γ ray will rarely Compton scatter, the first requirement of the analysis is a $88.97\pm 2\sigma$ keV event in one detector segment. External coincidences then require that this 88.97 keV γ ray is the only event in its clover detector and a 1857.4 keV γ ray is detected in the opposing detector. Given the higher energy of the 1857.4 keV γ ray, both addback and singles events are included in the search. Internal coincidences require the 1857.4 keV γ ray to be observed in a segment of the same clover and no triggers in the remaining six clover segments. Addback is not attempted for internal coincidences. The most stringent limits are found by including both internal and external coincidences. The ROI spectra found from the sum of internal and external coincidences is shown in Fig. 3.

B. To the 1952.4 keV state

The decay sequence for the 1592.4 keV state of ^{156}Gd is shown in Fig. 4. A 709.9+1242.5 keV γ-ray coincidence is produced in 44.7% of decays. The only other intense decay mode results in three coincidence γ rays with a branching ratio of 46.0%.

As the efficiency measurements were performed with two γ-ray coincidences, the two γ-ray decay will dictate

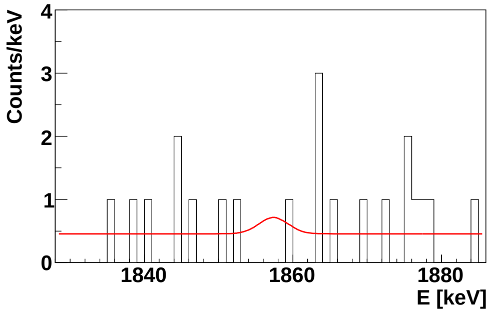

FIG. 3. (Color online) The ROI spectra for *ECEC* to the 1946.4 keV state of ^{156}Gd including both runs No. 1 and 2. Events in coincidence with 88.97 keV are shown. The red curve shows the background level and the minimum detectable signal, for a peak at 1857.4 keV, at the 90% confidence level.

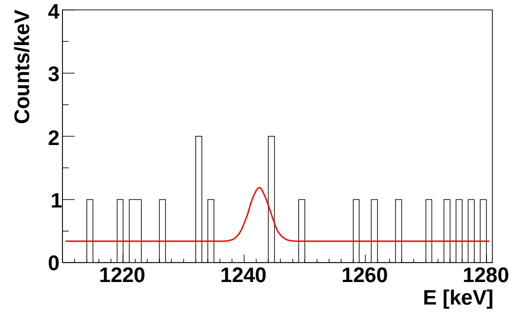

FIG. 5. (Color online) The ROI spectra for *ECEC* to the 1952.4 keV state including both runs No. 1 and 2. Events in coincidence with 709.9 keV are shown. The red curve shows the background level and the minimum detectable signal, for a peak at 1242.5 keV, at the 90% confidence level.

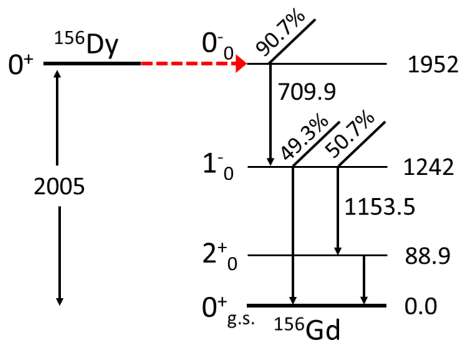

FIG. 4. (Color online) Decay scheme for the 0^-_4 1952.4 keV state of ^{156}Gd following *ECEC* to a resonant state. Only the most intense transitions are shown, while all other transitions have a branching ratio $< 3.8\%$.

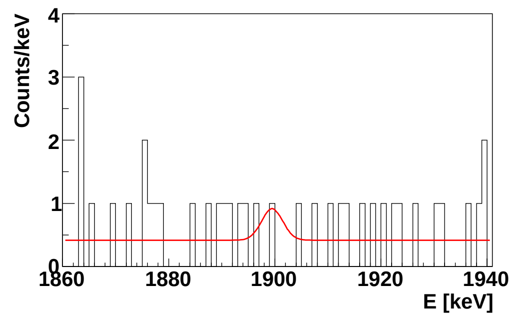

FIG. 6. (Color online) The ROI spectra for *ECEC* to the 1988.5 keV state including both runs No. 1 and 2. Events in coincidence with 88.97 keV are shown. The red curve shows the background level and the minimum detectable signal, for a peak at 1899.5 keV, at the 90% confidence level.

the analysis cuts. For this decay, the energy of both coincident γ rays is high enough that a significant portion will Compton scatter between clover segments. As such, the analysis procedure differs slightly from the one outlined in the previous section. External coincidences search for the 709.9+1242.5 keV coincidence between the two clover detectors operating in both singles and addback mode. Internal coincidences, once again, are between two detector segments of the same clover with no addback corrections made. This same analysis procedure is used for the other ROIs with two coincident γ rays above 400 keV.

The results of this analysis procedure are shown in Fig. 5. This analysis procedure does not intrinsically distinguish the two and three γ-ray decay modes from the 1952.4 keV state. For example, it is possible that the 1153.5 and 88.97 keV γ rays are detected in one clover then re-interpreted as a 1242.5 keV addback event. This possibility increases the experimental sensitivity of this ROI by including an additional decay mode and will be discussed in Sect. III F.

C. To the 1988.5 keV state

This nuclear state of ^{156}Gd is of particular interest because it is the only 0^+ state available for a resonant *ECEC* transition. Somewhat unfortunately, the state suffers from a dearth of nuclear data. No data is present on the possible decay modes from this state. Although the nature of the excitation will dictate the decay modes, it is reasonable to assume that the $0^+_4 \rightarrow 2^+_0 \rightarrow 0^+_{g.s.}$ transition will be one of the strongest, if not the most intense, transition. This is true for the other excited 0^+ states in ^{156}Gd. The decay scheme is similar to that of Fig. 2, except that the $0^+_4 \rightarrow 0^+_{g.s.}$ transition is forbidden. A search for events matching this decay mode focus on an 1899.5 + 88.9 keV γ-ray coincidence.

The analysis was performed identically to that of the 1946.4 keV state outlined in Sec. III A, with the 1857.4 keV ROI replaced with 1899.5 keV. The results are shown in Fig. 6.

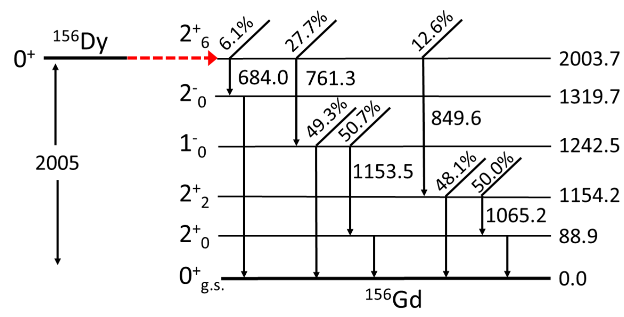

FIG. 7. (Color online) Decay scheme for the 2^+_6 2003.7 keV state of ^{156}Gd following *ECEC* to a resonant state. Only the most intense two γ-ray transitions are shown, while all other two γ-ray transitions have branching ratio $< 0.5\%$. The three γ-ray transitions associated with these two γ-ray transitions are also shown.

D. To the 2003.7 keV state

The 2^+_6 state of ^{156}Gd has a more complicated decay scheme than the other studied states. The state will decay to one of six different states, with the most intense decay sequence only accounting for 23% of all decays. As our efficiency measurements were performed for two coincidence γ rays, we limit ourselves to those cases, all of which are shown in Fig. 7. Unfortunately, the three decays producing only two γ rays have a combined branching ratio of 25.8%.

The procedure outlined in Sec. III B is again followed for these three decay modes. The 684.0+1319.7, 761.3+1242.5, and 849.6+1154.2 keV coincidences are investigated, with the results shown in Fig. 8. After the addition of sample No. 2, the background rate for the decay modes progressing via the 1242.5 and 1154.2 keV states was found to have an increased background. It was realized that the internal coincidence channel was responsible for the majority of the background increase. For the case of the decay to the 2^+_2 1154.2 keV state, the background rate was found to be sufficiently high that a better limit could be obtained by only including external coincidences. In this case, the loss in efficiency is compensated by the decreased background.

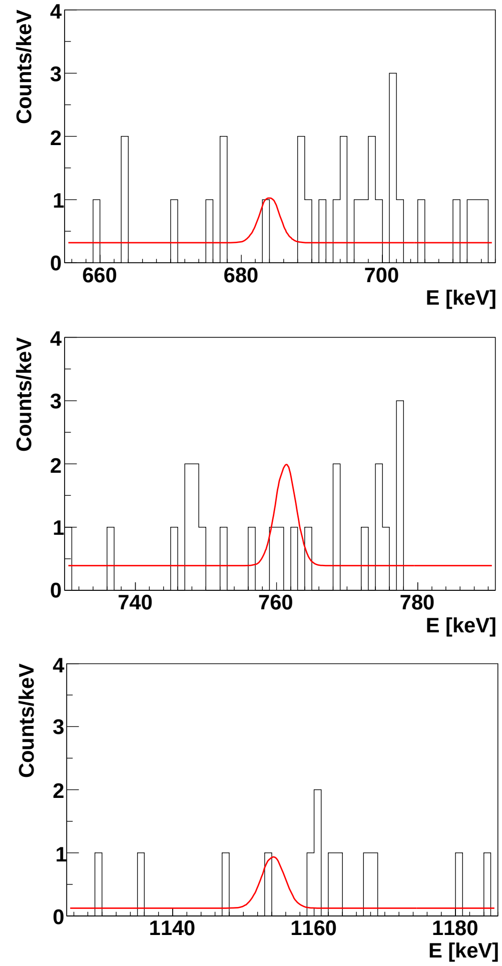

FIG. 8. (Color online) The ROI spectra for *ECEC* to the 2003.7 keV state including both runs No. 1 and 2. Events are shown in coincidence with 1319.7, 1242.5, and 849.6 keV respectively. The red curve shows the background level and the minimum detectable signal at the 90% confidence level.

E. Coincidence efficiency

In order to measure the coincidence efficiency of the apparatus, a ^{102}Rh source was used. This source was produced using the ^{102}Ru$(p,n)^{102}$Rh reaction with 5 MeV protons at the TUNL tandem accelerator. The source was 0.165 cm in diameter and 0.142 cm in height with an activity of 1.26 ± 0.04 kBq. The efficiency data were analyzed using the same analysis code as was used for the ^{156}Dy analysis. Only the ROI and detector resolution were changed to accurately reflect the run conditions.

This procedure produced efficiency data for the internal coincidences of both clover detectors, the external coincidences, and the addback coincidences for the ^{102}Rh ROI. The coincident detection efficiency was found to peak at the origin, and is relatively constant from $-1.5 < x < 1.5$ cm, as shown in Fig. 9. This motivated the size and placement of the Dy_2O_3 samples. As segment $c13$ was omitted from the analysis, it was also omitted from the analysis of the efficiency data. This does not change the internal efficiency of clover two, but it does decease the total internal coincidence efficiency of clover one by approximately a factor of two and makes the efficiency asymmetric, as shown in Fig. 10. The external efficiency was also lower due to the omission of $c13$, although much less so than for the internal coincidences.

The final efficiency was calculated by integrating the two-dimensional efficiency, as shown in Fig. 10, over the physical sample size. The integration was performed for all three detection modes and both ^{156}Dy samples.

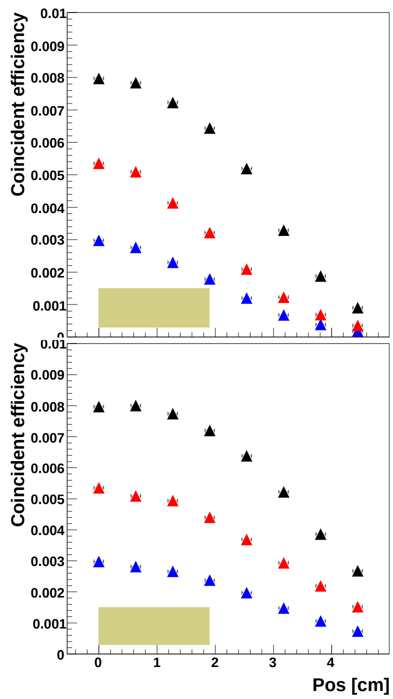

FIG. 9. (Color online) The coincident efficiency of the two-clover apparatus is shown along the two symmetry axes: diagonally across a crystal (top panel) and horizontally across two crystal edges (bottom panel). The efficiency is shown for the ^{102}Rh ROI and including $c13$. The maximum dimension of the ^{156}Dy sample is shown by the cream box, with the other dimensions of the rectangular sample being smaller.

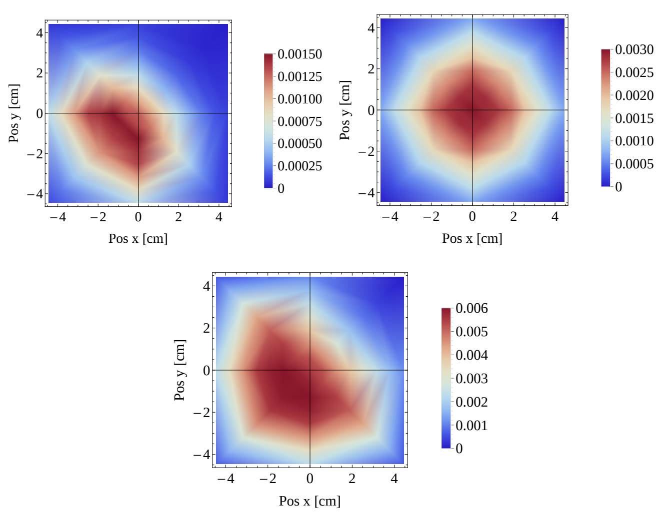

FIG. 10. (Color online) The coincident efficiency of the two-clover apparatus as a function of position with the omission of $c13$, located in the $(+x, +y)$ quadrant. The three panels show, clockwise from top left, the internal efficiency of clover one, the internal efficiency of clover two, and the external efficiency.

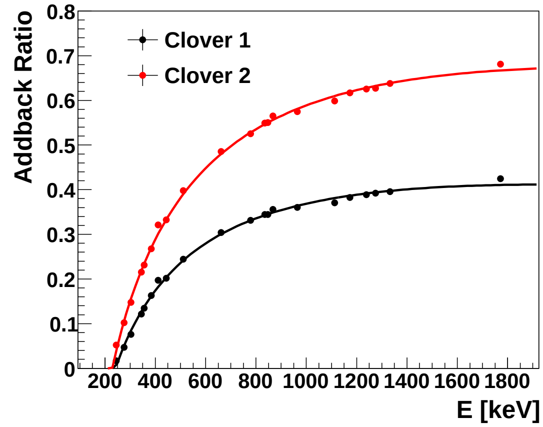

FIG. 11. (Color online) The addback ratio for the two clover detectors. Data are shown by the points and the functional fit is shown by the solid curves. The addback factor in clover one is noticeably lower due to the omission of segment three.

A number of corrections are necessary in order to apply these ^{102}Rh efficiency measurements to the possible ^{156}Dy decay modes.

1. *Energy dependence*

The energy dependence of the clover detector's efficiency was measured using a ^{152}Eu source. As one of the γ rays of interest for the $ECEC$ decay of ^{156}Dy has a relatively low energy, 88.97 keV, special care must be taken in calculating the efficiency of the detector at low energies. The clover detector has a 0.254 cm aluminum front window which will attenuate γ rays below $\approx$ 100 keV. In order to carefully account for this effect, GEANT4 simulations of the clover efficiency were performed at low energies. A correction factor to the total efficiency was calculated as a ratio of the coincidence energy for ^{102}Rh and the ^{156}Dy $ECEC$ ROI, as was performed in Ref. [7]. In calculating these corrections, the data points resulting from the GEANT4 simulations were only used for evaluation of the 88.97 keV efficiency. All other efficiencies were calculated using only the experimental data.

2. *Addback factor*

Following the procedure of Ref. [10], the addback efficiency may be written as the detector efficiency in singles mode times an addback factor, $f(E)$. The addback factor $f(E)$ was measured using several point sources and is shown in Fig. 11. As in Ref. [10], the addback factor is fit to a function, quadratic in $\log(E)$ in order to interpolate $f(E)$.

The addback factor is typically measured at a distance of 25 cm in order to prevent accidental summing of coincident γ rays. The experiment on ^{156}Dy, however, was conducted at a distance of 0.18 cm. Accordingly, $f(E)$ was measured at 25 cm using a variety of sources, and at 0.18 cm using sources producing single γ rays and the ^{102}Rh source. These measurements were confirmed by GEANT4 simulations. The addback factor was found to be 25 to 35% larger at 0.18 cm than at 25 cm, varying from 600 to 2000 keV.

3. Target attenuation

As the samples were very small and stored in polyethylene bags, the γ-ray attenuation by the sample itself is expected to be very small. The target attenuation was calculated using GEANT4. The samples were modeled in GEANT4 and events were simulated with and without the sample present. As expected, the attenuation was relatively small, $\approx 1-2\%$, for all decay modes with high-energy γ rays. The two decay modes producing the 88.97 keV γ ray, however, show a sizable attenuation factor: $\approx 14.2\%$ for run No. 1 and $\approx 28.9\%$ for run No. 2. This correction factor was calculated separately for internal and external coincidences and for both runs.

4. Detector separation and source geometry

The separation distance between the detectors was kept as small as possible in order to maximize the solid angle covered by the detectors. The same detector spacing, 0.18 cm, was used for the ^{102}Rh source measurements and for run No. 1 (including only sample No. 1). GEANT4 was utilized to calculate any difference in efficiency that occurred from the detector spacing and the physical extent of the ^{156}Dy sample. The insertion of sample No. 2 increased the distance between the detectors to 0.32 cm and resulted in a small decrease in efficiency, 3.32±0.01%, as calculated through the Monte Carlo simulation.

5. Angular dependence of coincident γ rays

As the efficiency measurements were performed using a $0^+ \rightarrow 2^+ \rightarrow 0^+_{g.s.}$ decay sequence, corrections must be made for the various decay modes of interest with different spin assignments. The effect was accurately modeled using GEANT4, as the angular distributions of the γ rays are set by theory. The other decay modes studied were more isotropic than the $0^+ \rightarrow 2^+ \rightarrow 0^+_{g.s.}$ decay mode and shifted efficiency from the external coincidences to the internal coincidences, with a small change in the total efficiency, $< 4\%$.

6. Final efficiency

The final efficiency for each of the decay modes is summarized in Table II. These results include all of the previously mentioned corrections. Additionally, the systematic error budget is shown in Table III, which contains the uncertainties associated with each of the previous corrections.

TABLE II. The final efficiency, in [%] for the ^{156}Dy ROIs for both runs. The external coincidence, internal coincidence, and the total (combined) efficiency are all given.

J^π	γ_1	γ_2	Run No. 1			Run No. 2		
	[keV]	[keV]	ϵ_{ext}	ϵ_{int}	ϵ_{tot}	ϵ_{ext}	ϵ_{int}	ϵ_{tot}
1^-_2	1857.4	88.97	0.597	0.335	0.933	0.478	0.277	0.755
0^-_0	709.9	1242.5	0.373	0.135	0.508	0.353	0.131	0.484
0^+_4	1899.5	88.97	0.639	0.275	0.915	0.523	0.228	0.751
2^+_6	684.0	1319.7	0.362	0.142	0.504	0.340	0.136	0.476
2^+_6	761.3	1242.5	0.348	0.141	0.489	0.326	0.136	0.461
2^+_6	849.6	1154.2	0.343	0.131	0.474	0.323	0.128	0.451

TABLE III. The systematic error budget for the *ECEC* decay of ^{156}Dy to the 1946 keV state. Note that uncertainty on the energy dependence, attenuation, and addback correction factors are energy dependent and vary for each ROI.

Uncertainty contribution	Percent error
Calibration of ^{137}Cs source	3.1 %
^{102}Rh efficiency measurements	1.2 %
Detector and source geometry	3.0 %
Angular dependence of γ rays	1.20 %
Addback correction factors	2.9 %
Energy dependence correction factor	0.5 %
Attenuation correction factor	0.20 %
Dead time	0.20 %
Uncertainty in ^{102}Rh half-life	0.82 %
Total uncertainty	5.6 %

F. Contributions from three-γ decays

As has already been mentioned, the decays to the 1952.4 and 2003.7 keV states have significant branching ratios for transitions that produce three coincident γ rays. It is possible for a clover detector to detect two of these γ rays in coincidence and reconstruct them as an addback event with the same energy as one of the two original γ rays of interest. This is a signal event that will pass the analysis procedure utilized. As the apparatus will detect both of these decay modes, this effect will further increase the experimental sensitivity. The efficiency of a triple coincidence is considerably lower than that of a double coincidence. The three γ-ray efficiency was simulated using GEANT4. Using these simulations, the ratio $\epsilon_{3\gamma}/\epsilon_{2\gamma}$ was calculated. This ratio is preferred as it minimizes systematic uncertainties arising in the simulations. The ratio is given in Table IV for the sum of internal and external coincidences. The ratio was found to vary around $\sim 0.22-0.27$ for external coincidences. Interestingly, even though no addback was utilized for

TABLE IV. The contributions from the three-γ decay mode into the two-γ ROI.

J^π	γ_1 [keV]	γ_2 [keV]	γ_3 [keV]	$\epsilon_{3\gamma}/\epsilon_{2\gamma}$ Run No. 1	$\epsilon_{3\gamma}/\epsilon_{2\gamma}$ Run No. 2
0_0^-	709.9	1153.5	88.97	0.228 ± 0.003	0.190 ± 0.003
2_6^+	761.3	1153.5	88.97	0.226 ± 0.003	0.192 ± 0.003
2_6^+	849.6	1065.2	88.97	0.252 ± 0.004	0.212 ± 0.003

TABLE V. For each $ECEC$ decay mode studied, the ROI, effective branching ratio $f_{b,eff}$, number of observed events n_{obs}, number of background events n_{bkgd}, the Feldman-Cousins upper limit N_d, the Feldman-Cousins sensitivity N_s, and the systematic uncertainty σ_{syst} are given.

J^π	γ_1 [keV]	γ_2 [keV]	$f_{b,eff}$	n_{obs}	n_{bkgd}	N_d	N_s	σ_{syst}
1_2^-	1857.4	88.97	0.578	1	4.12	1.28	4.86	5.6%
0_0^-	709.9	1242.5	0.531	2	2.38	3.55	4.12	5.7%
0_4^+	1899.5	88.97	1[a]	2	3.76	2.49	4.72	5.6%
2_6^+	684.0	1319.7	0.061	1	1.92	2.59	3.87	5.7%
2_6^+	761.3	1242.5	0.163	4	2.74	5.86	4.29	5.7%
2_6^+	849.6	1154.2	0.076	1	0.99	3.37	3.27	5.7%

[a] As this branching ratio has not been measured, it is assumed to be 1.

TABLE VI. The final half-life limits for the $ECEC$ decay of ^{156}Dy to excited states at the 90% confidence level. Both the confidence limit, the experimental sensitivity, and the previous experimental limit are given

J^π	E [keV]	Lim $T_{1/2}$ [yr] This work C.L.	Lim $T_{1/2}$ [yr] This work Sensitivity	Lim $T_{1/2}$ [yr] Previous limit [14]
1_2^-	1946.4	1.0×10^{18}	2.8×10^{17}	9.6×10^{15}
0_0^-	1952.4	2.2×10^{17}	1.9×10^{17}	2.6×10^{16}
0_4^+	1988.5	9.5×10^{17}[a]	5.0×10^{17}[a]	1.9×10^{16}
2_6^+	2003.7	6.7×10^{16}	-	3.0×10^{14}

[a] This limit is calculated for the $0_4^+ \rightarrow 2_0^+ \rightarrow 0_{g.s.}^+$ decay mode and assumes a branching ratio of 1. If the branching ratio is measured to be less than one, these values must be multiplied by the new branching ratio.

internal coincidences, the three γ-ray decay can still be observed in the internal coincidence ROI due to coincident summing. This contribution is less probable and, as expected, has a ratio of $\sim 0.10 - 0.12$.

The improvement due to this effect depends on the branching ratio of the decay. As such, the correction was not included in the above efficiency values. When calculating limits on the half-life, the product of the branching ratio f and the efficiency ϵ is summed over all decay modes. Assuming two possible decay modes, the effect is rewritten

$$\sum_{n=2\gamma,3\gamma} f_n \epsilon_n = \epsilon_{2\gamma}\left(f_{2\gamma} + f_{3\gamma}\frac{\epsilon_{3\gamma}}{\epsilon_{2\gamma}}\right) . \quad (2)$$

This factor is used to calculate the half-life limits presented in the following section. An additional 6.0% systematic uncertainty is assigned to the efficiency ratio to account for the differences between the GEANT4 simulation and the measured efficiency. Incorporating these effects, the effective branching ratio from the 1952 keV state increases from 44.7% to 53.1%. For the two decays from the 2003 keV state that exhibit ternary decays, via the 1242 and 1154 keV states, the effective branching ratio is 16.3% and 7.35%, respectively. This is an increase over the naive branching ratios of 13.7% and 6.06%, respectively.

G. Limit setting

As no statistically significant counts were seen above background, lower limits were set using the formula

$$T_{1/2} > \frac{\ln 2 N_0 t f_b \epsilon_{2\gamma}^{tot}}{N_d} , \quad (3)$$

where N_0 is the number of nuclei, t is the exposure time, f_b is the effective branching ratio, $\epsilon_{2\gamma}^{tot}$ is the efficiency with all the corrections discussed in the previous section, and N_d is a statistical factor representing the number of counts above background to which the experiment is sensitive. N_d was calculated using the method of Feldman and Cousins [13] for a Poisson process and a 90% confidence level. The systematic uncertainty on the efficiency is included in limit setting at the 90% confidence level. In the case that the number of observed counts is less than the expected background, the Feldman-Cousins sensitivity is given in addition to the confidence limit. The sensitivity is only a function of the expected background and is the mean limit that would be measured by a collection of experiments with no true signal.

The results of the analyses are summarized in Table V. The curves in Figs. 3, 5, 6, and 8 show the expected signal using the 90% Feldman-Cousins confidence limit given here. These results are for the sum of run No. 1 and 2, which produces better limits than either run alone. This represents a combined run time of 0.635 yr and a total exposure of 0.119 g·yr of ^{156}Dy. The Feldman-Cousins upper limit and sensitivity are both given at the 90% confidence level. As the 2_6^+ 2003.7 keV state has three separate two γ-ray transitions with a significant branching ratio, the results are listed for all three.

Final limits for resonant $0\nu ECEC$ are given in Table VI. In calculating these limits, it was assumed that the 0_4^+ state decays entirely through the 2_0^+ state, as discussed in Sec. III C. These limits may be easily updated, should the branching ratio be measured, by simply multiplying the limit by the measured branching ratio. The three decay modes from the 2003.7 keV state are summed together to present a single confidence limit. The results of this procedure are shown in Table VII.

TABLE VII. The half-life limits for the $ECEC$ decay of ^{156}Dy to the 2003.7 keV state at the 90% confidence level. The final limit is produced from the combined statistics of the three studied decay modes.

Decay sequence	Lim $T_{1/2}$ [yr]
$2_6^+ \rightarrow 2_0^- \rightarrow 0_{g.s.}^+$	3.4×10^{16}
$2_6^+ \rightarrow 1_0^- \rightarrow 0_{g.s.}^+$	3.9×10^{16}
$2_6^+ \rightarrow 2_2^+ \rightarrow 0_{g.s.}^+$	2.2×10^{16}
Combined	6.7×10^{16}

IV. CONCLUSIONS

The previous limits on $ECEC$ of ^{156}Dy were performed at Gran Sasso National Laboratory using a single 244 cm^3 coaxial HPGe detector [14]. A 322 g sample of ^{nat}Dy$_2$O$_3$ was counted for 2512 hours. This large sample was of natural abundance, 0.056%, amounting to 157 mg of ^{156}Dy. The limits produced by the current work represent a large improvement over these limits. The limit to the 1_2^- state is improved by a factor of 29, the 0_0^- state by a factor of 7.3, the 0_4^+ state by a factor of 26, and the 2_6^+ state by a factor of 220. This is much in part due to the higher efficiency of the two-clover apparatus and use of an isotopically enriched sample. The present work has a 36% larger sample when both samples are utilized. Furthermore, when using a large 322 g natural abundance sample, efficiency measurements must be performed over a large spacial extent and sizable efficiency corrections must be made for the self attenuation by the target. With the smaller, enriched samples used in the present work, the attenuation is much smaller and the detectors are able to cover a larger solid angle. Another concern in a single-detector experiment is the multiplicity of the γ cascade. In order to observe the full excitation energy, all of these γ rays must be emitted towards the detector. The present work covers close to 4π by surrounding the sample with two clover detectors. This allows for detection of back to back γ rays in addition to two forward going γ rays. Finally, a much higher signal-to-background ratio is achieved through the use of the $\gamma - \gamma$ coincidence.

The prefactor and nuclear matrix element for the decay to the 0_4^+ state are calculated in Ref. [4], which estimates a half-life of 2.89×10^{30} years for $\langle m_\nu \rangle = 1$ eV. As such, the current limits are not able to provide competitive limits on the neutrino mass or $ECEC$ matrix elements. Moreover, the current experimental uncertainties in the Q value for this decay mode will translate into a factor of three uncertainty in the decay half-life. The extreme sensitivity of the half-life on the Q value will inherently limit the accuracy of neutrino mass measurements performed with $0\nu ECEC$. A much larger sample mass is necessary in order to test the theory of Majorana neutrinos using resonant $0\nu ECEC$. ^{156}Dy samples are of course limited by the small natural abundance of this isotope.

Using the presented results, one can envision designing a large-scale $ECEC$ experiment. A large-scale experiment would necessitate enriched samples, which the present work shows can be produced without large radioactive backgrounds in the region of interest. The experiment would also greatly benefit from the background reduction provided by detection of coincident γ rays. This would be best accomplished using a segmented detector, as was done here, or another method of γ-ray tracking for position sensitivity. This would help distinguish Compton-scattered γ rays from signal events. Although the energy resolution of HPGe detectors is essential in the present work, a large-scale experiment would want to investigate a detector material containing Dy. A large-scale experiment, however, is not necessary until a viable resonant $0\nu ECEC$ candidate isotope is identified. The present two-clover apparatus has been proven to produce high-quality $ECEC$ half-life limits for ^{156}Dy with the ability to measure any candidate isotopes that may emerge with new precision mass measurements.

ACKNOWLEDGMENTS

This work was supported in part by the US Department of Energy, Office of Nuclear Physics under Grant No. DE-FG02-ER41033. The authors would like to thank R.B. Vogelaar and S.D. Rountree for their role in establishing and maintaining KURF. The authors would also like to thank Bret Carlin for his networking experience and construction of the remote liquid nitrogen fill system.

[1] Z. Sujkowski and S. Wycech, Phys. Rev. C **70**, 052501(R) (2004).
[2] R. G. Winter, Phys. Rev. **100**, 142 (1955).
[3] M. I. Krivoruchenko, F. Šimkovic, D. Frekers, and A. Faessler, Nucl. Phys. A **859**, 140 (2011).
[4] J. Kotila, J. Barea, and F. Iachello, Phys. Rev. C **89**, 064319 (2014).
[5] S. Eliseev *et al.*, Phys. Rev. C **84**, 012501 (2011).
[6] M. F. Kidd, J. H. Esterline, W. Tornow, A. S. Barabash, and V. I. Umatov, Nucl. Phys. A **821**, 251 (2009).
[7] M. F. Kidd, J. H. Esterline, S. W. Finch, and W. Tornow, Phys. Rev. C **90**, 055501 (2014).
[8] S. W. Finch and W. Tornow, Phys. Rev. C **92**, 045501 (2015).
[9] M. F. Kidd, J. H. Esterline, and W. Tornow, Phys. Rev. C **78**, 035504 (2008).
[10] G. Duchêne *et al.*, Nucl. Instrum. Methods A **432**, 90 (1999).
[11] P. Finnerty *et al.*, Nucl. Instrum. Methods A **642**, 65 (2011).

[12] M. W. Ahmed, C. R. Howell, and A. S. Crowell, "Coda at tunl (c@t) and the tunl real-time analysis package (trap) version 03.a," (2014), [Online; accessed 23-January-2014].
[13] G. J. Feldman and R. D. Cousins, Phys. Rev. D **57**, 3873 (1998).
[14] P. Belli *et al.*, J. Phys. Conf. Ser. **375**, 042024 (2012).